PAPER

Check for updates

High resolution light-based 3D printing of a bio-sourced monomer with tuneable depolymerisation

Pia S. Klee, [ID] Samantha O. Catt, [ID] Lea Sielaff and Eva Blasco [ID] *

Light-based 3D printing has historically relied mainly on the photopolymerisation of (meth)acrylate-based inks. However, exploring new chemistries that include heteroatom-containing linkages can increase depolymerisation options and results in more sustainable inks. Bio-based dithiolanes are an emerging class of alternative printable materials. Herein, we present a dithiolane-based ink and analyse its printing performance across scales—from macroscale structures fabricated *via* digital light processing to microscale features achieved through two-photon laser printing. We demonstrate the successful fabrication of complex 3D structures with fine feature resolution, highlighting the material's suitability for microscale applications. Moreover, we incorporate a thermally latent base to enable controlled thermal depolymerisation, which is effective across both printing scales. This work represents the first example of targeted depolymerisation in microprinted structures using an embedded latent base, offering a novel and sustainable (meth)acrylate-free strategy.

Introduction

In recent years 3D printing has emerged as a continuously evolving fabrication technique for polymeric materials, spanning a range of applications from everyday objects to microscale structures.[1–3] Due to the low waste generation and on demand fabrication style, 3D printing can be considered an inherently sustainable manufacturing technique.[4–6] However, the materials used are a large factor when evaluating its environmental impact, and must be shifted towards bio-based feedstocks with end-of-use options.[7] In particular, light-based 3D printing is a commonly employed method to print materials at both the macro- and micro-scale leading to high resolution structures with fast fabrication speeds.[7,8] At the macro-scale, digital light processing (DLP) is a favoured technique,[9] meanwhile, on the micro-scale, two-photon laser printing (2PLP) is typically used. Both techniques rely on a photopolymerisation process. While in DLP, one-photon polymerisation takes place, in 2PLP the photopolymerisation is initiated by the non-linear absorption of two or more photons by the same chromophore, leading to high spatial resolution.[10]

While there have been efforts to create inks for light-based 3D printing on the basis of renewable feedstocks, commonly their photopolymerisation process still relies on the radical polymeris-

*Institute for Molecular Systems Engineering and Advanced Materials,
Im Neuenheimer Feld 225, 69120 Heidelberg, Germany.
E-mail: eva.blasco@uni-heidelberg.de*

ation of (meth)acrylate groups, including a photoinitiator to initiate the reaction.[11–13] Despite the benefits of easy processing, fast polymerisation, and high versatility, the significant drawback of the resulting polymeric networks having a carbon backbone, remains. This limitation in the types of linkages that are incorporated into the 3D printed structures, results in networks that are hard to degrade and limits their end-of-use options, in turn contributing to the ever-growing plastic waste problem.[14]

There has been a growing interest in finding alternative photopolymerisable units, that could replace the current (meth)acrylates and be depolymerised through integrating heteroatomic bonds into the formed polymeric network. Recent examples of alternative photochemistries explored for light-based printing include thiol–ene/yne networks and reversible cycloadditions.[15–18] Of these systems, few have been successfully established on the micro-scale.[19] Despite promise as alternatives to traditional (meth)acrylates, the photopolymerisation is often less efficient and still poses challenges in full depolymerisation.

To that end, the use of 1,2-dithiolane rings, found in the naturally sourced lipoic acid (LA), has become a prospective alternative moiety for applications in light-based 3D printing. Upon irradiation, a ring opening reaction of strained disulfide rings leads to new linear disulfide bonds, thus forming a dynamic covalent network. Notably, these materials are readily depolymerisable and have been shown to be printable without photoinitiators, which are often toxic.[20] Recent works pioneered by Dove and co-workers focus on macroscale 3D printing using DLP.[21–25] This system, as a novel alternative photochemistry is interesting as an alternative to the commonly

used acrylates, however it remains in its early stages, and it has only been scarcely explored for micro-scale 3D printing.[24]

When exploring depolymerisation strategies, latent bases have emerged as a promising method. They offer the possibility to trigger exchange reactions in dynamic covalent systems upon their release following exposure to a stimulus such as light or temperature. This property can in turn be used to tune the depolymerisation conditions of a polymer network from within.[26,27] Schlögel and co-workers have demonstrated applications of this in DLP printed materials, through the incorporation of thermally latent bases into printable inks.[28] The added flexibility of being able to change the conditions at which a network depolymerises is not only relevant for macro-scale 3D printed structures to enhance recycling options, but transferring this concept to micro-scale printing is also of great interest. The unique combination of the potential for tuneable depolymerisation using latent bases, with the dynamic nature of dithiolane networks remains unexplored, presenting an intriguing system with high flexibility when applied to light-based 3D printing across multiple length scales.

To this aim, we introduce a depolymerisable dithiolane-based ink that enables high-resolution light-based 3D printing on both the macro- and micro-scale (Fig. 1a). The ink consists solely of a difunctional crosslinker built from biobased starting materials – lipoic acid and ethylene glycol – that can be photopolymerised without any further additives. Importantly, tuneable depolymerisation of the 3D printed material using a latent base is successfully introduced, allowing for modification of the thermal depolymerisation behaviour of the printed structures (Fig. 1b). After validating the ink's printability on the macro-scale by DLP printing, we thoroughly investigate its performance for micro-scale 2PLP printing. Finally, we successfully adapt the concept of latent base activated depolymerisation to be applied in micro-scale 3D printed structures for the first time. This innovative adaptation of latent bases as depolymerisation stimuli allows for the creation of a sustainable multi-scale 3D printing approach, opening up exciting avenues for a broad range of potential applications.

Results and discussion

Macro-scale 3D printing

To develop a sustainable ink based on 1,2-dithiolane rings for DLP printing, biobased starting materials were deliberately chosen to enable the synthesis of a photopolymerisable crosslinker without reliance on petroleum-derived compounds. Lipoic acid (LA), a naturally occurring organosulfur compound, and ethylene glycol (EG), a diol accessible from biomass-derived feedstocks, served as the primary building blocks for the envisioned ink system. The bifunctional crosslinker was synthesised through Steglich esterification of EG and two units of LA, however, there have been recent reports of a more sustainable synthetic route.[29] The product, further referred to as LA-EG-LA, was obtained as a yellow oil in a high yield. Being in liquid form at room temperature makes this crosslinker very suitable for light-based 3D printing, as no additional solvent is required to solubilise the material.

In a next step, the one-photon photopolymerising behaviour of the synthesised material was investigated to assess its suitability for DLP 3D printing. Photopolymerisation properties were examined by measuring the cure depth with respect to exposure time with a fixed wavelength and light intensity when projecting a 2 mm circle onto a droplet of material. A 405 nm LED was chosen as this led to faster polymerisation than 385 nm (Fig. S6). The ink polymerised in a timeframe suitable for 3D printing without the need for a photoinitiator. Instead, the light directly causes the dithiolanes to undergo a ring opening reaction forming a network containing linear disulfide bonds.[21] Following the model established by Jacobs,[30] the results were plotted in the form of working curves, from which the critical energy, at which photopolymerisation starts to occur, was calculated and lies at 192 mJ cm^{-2} (Fig. 2a). Once suitable printing parameters had been established, a flower could successfully be printed as an exemplary 3D structure (Fig. 2b) at 405 nm and an intensity of 55 mW cm^{-2} with a layer thickness of 100 μm and an irradiation time of 41 s per layer. The ink achieved high print-
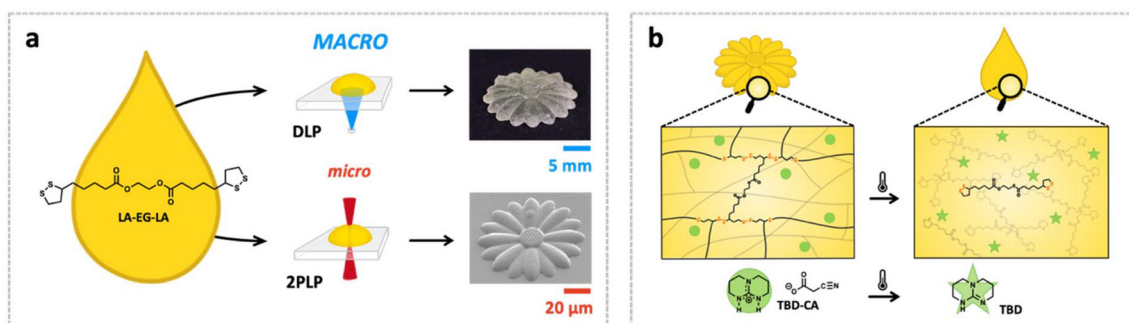

Fig. 1 (a) 3D printing process on the macro- and micro-scale: a difunctional crosslinker (LA-EG-LA) synthesised from bio-based starting materials – lipoic acid and ethylene glycol – is used without the need of additional additives for 3D printing using digital light processing (DLP) and two-photon laser printing (2PLP). (b) Latent base activated depolymerisation of 3D printed structures is performed by thermal activation, enabling controlled depolymerisation across both printing scales.
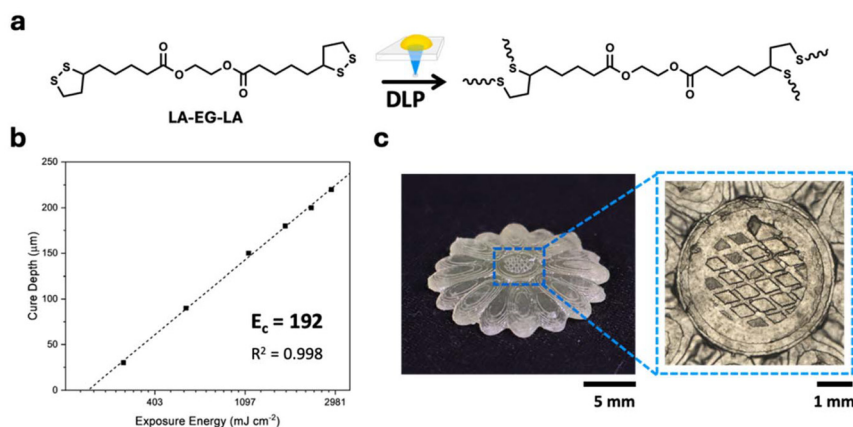
Fig. 2 (a) Photopolymerisation reaction of LA-EG-LA for the formation of a polymer network during the DLP printing process. (b) Jacobs working curves of LA-EG-LA with an LED at 405 nm. (c) 3D printed flower printed with a layer thickness of 100 μm and a light intensity of 55 mW cm^{-2}, light microscope image showing the highly detailed centre of the 3D printed flower.

ing resolution, as demonstrated by the small, detailed pattern at the centre of the printed flower (Fig. 2c). The printed flower displays very little shrinkage with the measured width of 17 mm being equal to that of the 3D model. The diamond shaped details at the centre of the flower can be seen in Fig. 2c. The diamonds of the 3D model have a length of 75 μm which is close to that measured of the printed structure of 70 μm, thus demonstrating the high fidelity.

Incorporating a latent base

Once the printing conditions were established for the macro-scale 3D printing, the depolymerisation conditions of the printed macrostructures were investigated. It is known that networks based on dithiolanes can easily be depolymerised, for example, with organic bases such as diazabicycloundecen (DBU) and triazabicyclodecene (TBD),[31] which we confirmed for our 3D printed networks (Fig. S3). Here, we go one step further and increase the flexibility of the depolymerisation conditions by the incorporation of a latent base, which can be released upon exposure to an external trigger. To this aim, TBD was chosen as the active base, which is 'deactivated' by forming a salt with cyanoacetic acid (CA), giving the 'latent' form. Upon heating to approximately 150 °C the active base can then be released again, while the anion decomposes.[28] TBD-CA was incorporated into the ink by dissolving 5 wt% in LA-EG-LA. The photopolymerisation behaviour with the latent base–containing ink showed that the printability is very similar to the pure ink containing only the crosslinker (see Jacobs working curves Fig. S5).

To demonstrate the impact the incorporation of the base has on the depolymerisation conditions, bars (20 × 3 × 2 mm) were 3D printed with and without TBD-CA and ground into a fine powder. The powders resulting from the two printed materials were heated to 150 °C at which the TBD is released. After 10 min a clear difference can be seen (Fig. 3). While the blank sample remains solid, the sample containing the latent base depolymerises into a reddish liquid. The discolouration

that can be observed likely stems from some decomposition of the thiols.

Additionally, the material properties were characterised by dynamic mechanical analysis (DMA) of 3D printed samples without and with latent base (Table 1). The printed material using just the crosslinker LA-EG-LA exhibits a T_g of 22.8 °C determined by the maximum of tan δ and a storage modulus (E') of 41 MPa at room temperature. When compared with the 3D printed material including the latent base, a slight increase in T_g (24.9 °C) can be observed but still lies within a comparative range. The rubbery plateau is reached after approximately at 20 °C after the T_g and here E' lies at 16 MPa for the pure LA-EG-LA samples and 13 MPa for the samples containing the latent base. A single, relatively narrow peak of tan δ was found indicating the homogeneity of the material, which was not impacted by the addition of the latent base (Fig. S7). The DMA measurements also show that the sample containing the latent-base starts to break at 130 °C due to the depolymerisation that is caused by the activation of the latent base, while the blank sample remains stable until higher temperatures.

Micro-scale 3D printing

After establishing the presented system on the macro-scale, we focus on micro-scale printing using 2PLP. Here, the implementation of latent bases to achieve tuneable depolymerisation conditions is of particular interest, since working on the micro-scale severely limits the processing options for the depolymerisation of printed structures.

Using the same ink consisting of only the LA-EG-LA crosslinker, the two-photon polymerisation capabilities were explored for micro-scale printing utilising a 2PLP commercial printer with a 780 nm laser. A dose test was performed consisting of pillars with a diameter of 20 μm and height of 5 μm printed with conditions ranging from scanning speeds of 2 to 20 mm s^{-1} and laser powers from 10 to 32 mW. The range of printability was found to be broad over a window of scan speeds and laser powers as illustrated by pillars highlighted in
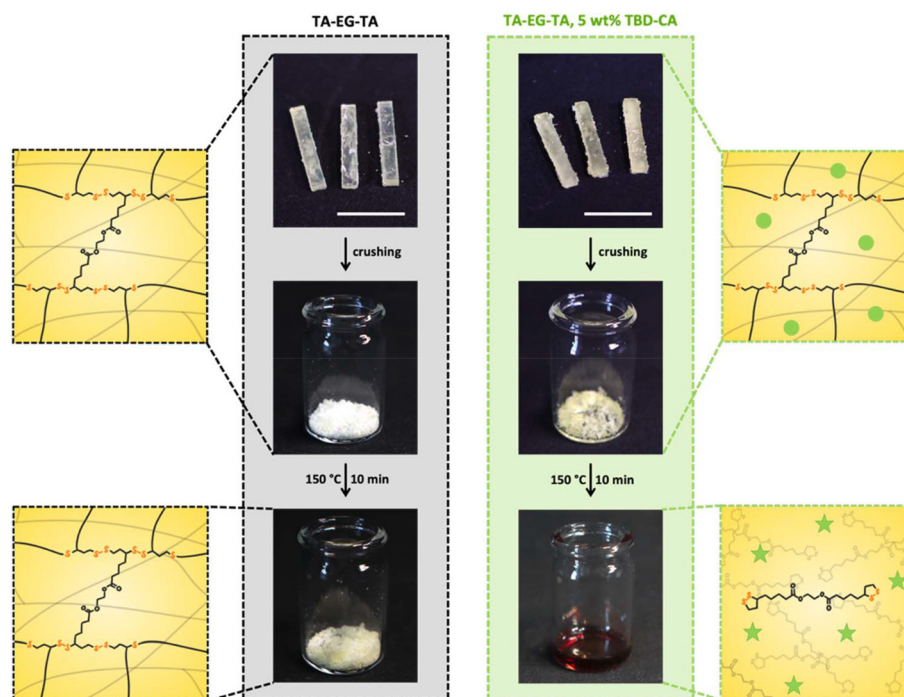
Fig. 3 Comparison of depolymerisation behaviour of 3D printed LA-EG-LA without (left/black) and with (right/green) TBD-CA after crushing with a mortar and heating to 150 °C for 10 min with illustration of the network depolymerisation by activation of TBD-CA, scalebar = 10 mm.

Table 1 Mechanical characterisation by DMA of 3D printed structures with and without the addition of 5 wt% TBD-CA

3D printed material	$T_g{}^a$ (°C)	E'^b at 25 °C (MPa)	E'^b at 50 °C (MPa)
LA-EG-LA	22.8	41.3	15.6
LA-EG-LA + TBD-CA	24.9	43.4	13.1

^{a} Glass transition temperature (T_g) determined from maximum of tan δ. ^{b} Storage modulus (E') at room temperature; (E') of rubbery plateau.

red (Fig. 4a). The SEM image shows that the ink is printable both at high scanning speeds up to 20 mm s^{-1} with high laser powers as well as low scanning speeds with lower laser powers. In particular, employing high scanning speeds and laser powers yields good results, which outperforms other new chemistries that have been developed for multiphoton printing and is on par with commercial inks.[19] High scan speeds allow for fast build times which broadens the inks potential for applications where larger arrays are required. To demonstrate its versatile printability on the micro-scale, more complex geometries were also printed with LA-EG-LA (Fig. 4b). The flower (diameter = 80 μm) displays the intricate pattern at the centre, demonstrating fine feature resolution, while the bucky ball (diameter = 20 μm) and 'benchy' (length = 25 μm) both show that printing more complex 3D microstructures, even with hollow features and overhangs, is also possible. LA-EG-LA is therefore proven to not only be printa-

ble through one-photon polymerisation methods leading to macroscopic structures but can also be printed through a multiphoton approach, without the need for an additional photoinitiator.

The dose test gave an initial insight into the impact of the printing parameters, which was further investigated by 3D printing a honeycomb geometry at four different laser powers, while keeping the scanning speed constant at 15 mm s^{-1} (Fig. 4c). When measuring the size of the hexagonal internal micropores as a reference, the same trend that was indicated in the dose test is present (Fig. 4d). Initially, increasing laser powers leads to an increase in the size of the structures and therefore the hexagonal pores, likely due an increasing network density and therefore lower shrinkage. From 27.5 to 30 mW the pore size then decreased again which could be rationalised by the higher laser power leading to overpolymerisation, which can also be seen in a more pronounced way at high laser powers in the dose test. Overall, these results show that the printing parameters can be easily fine-tuned depending on the desired outcome or structure. For deeper insight into the network formation, nanoindentation was used to investigate the mechanical properties of microprinted pillars, as DMA measurements are not possible on the micro-scale. Again 15 mm s^{-1} was chosen as a constant scanning speed. The resulting reduced elastic modulus (E_R) was between 7.0–10.5 MPa for the measured materials (Table S1), which lies in the same range of the macroscopic DMA measurements. To further validate the comparability of the nanoindentation and DMA measurements, the E_R of a macroscopic sample (pro-
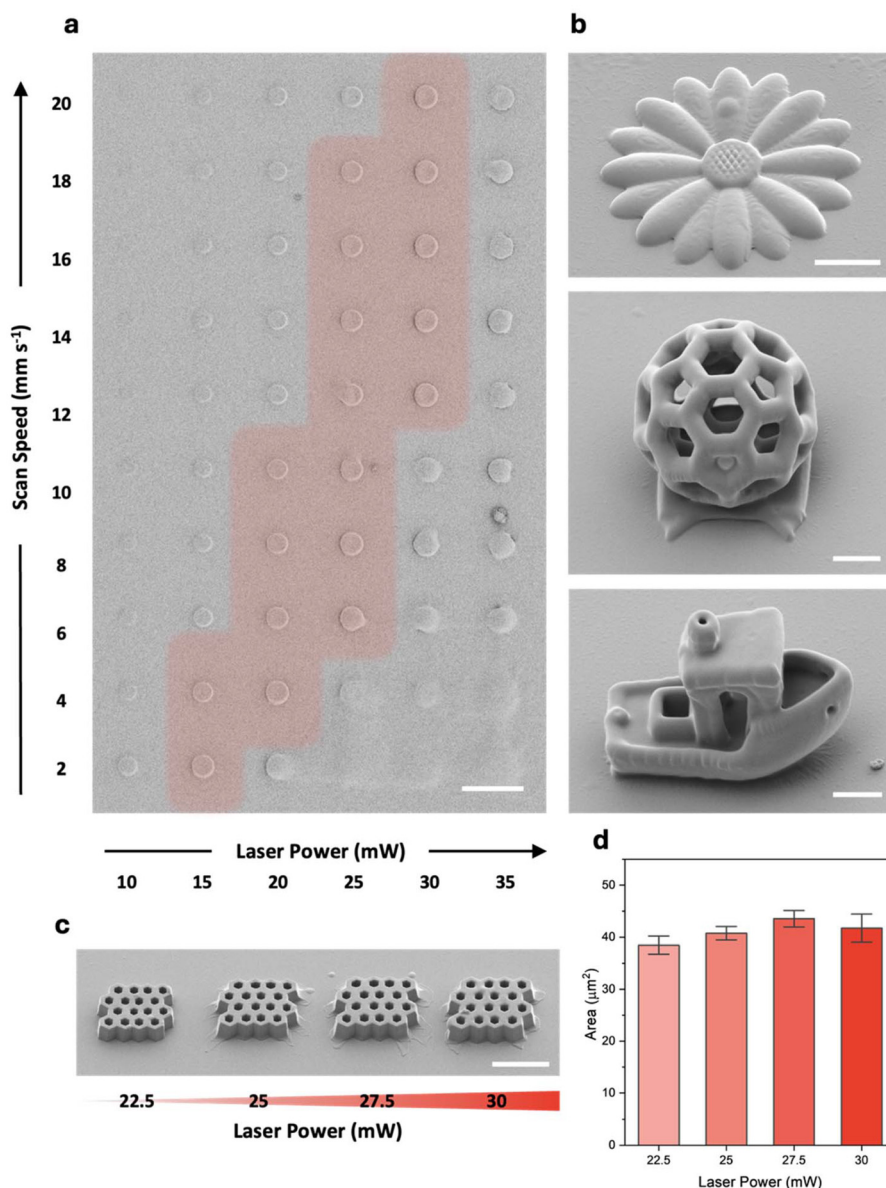
Fig. 4 (a) SEM image of a dose test printed with pure LA-EG-LA with a scan speed ranging from 2 to 20 mm s^{-1} with a step of 2 mm s^{-1} and laser power ranging from 10 to 35 mW with a step of 5 mW, printable range highlighted in red, scalebar = 50 μm. (b) SEM images of complex geometries printed with a scan speed of 15 mm s^{-1} and laser power of 22.5 mW (flower) scalebar = 20 μm, 12 mm s^{-1} and 30 mW (buckyball) scalebar = 5 μm, and 20 mm s^{-1} and 30 mW (benchy) scalebar = 5 μm. (c) SEM images of honeycomb structures printed at four different laser powers ranging from 22.5 to 30 mW with a step of 2.5 mW and a constant scan speed of 15 mm s^{-1}, scalebar = 50 μm. (d) Average pore size of the honeycomb with respect to laser power.

duced by DLP) was measured by nanoindentation and resulted in a comparable value at room temperature (24.8 ± 1.4 MPa) to the storage modulus obtained from DMA (41.3 MPa).

Latent base depolymerisation of 3D microstructures

To explore the depolymerization of 3D microstructures, the latent base was also introduced into the micro-scale printing process. Due to the nature of the microprinting process, which includes a development step where the remaining ink is washed away with a solvent, it was more advantageous to introduce the latent base in a post-processing "doping" step rather than including it in the ink. This also negates the risk that any dissolution problems could impact the 3D printing process, which is more sensitive to variations in the ink formulation than on the macro-scale, particularly when avoiding the introduction of a solvent component. First, woodpile arrays were 3D printed, and the resulting structures were submerged in a concentrated solution of TBD-CA in isopropanol for 30 min (Fig. 5a). The incorporation of the latent base in the 3D printed microstructures was monitored by FTIR spectroscopy, where an additional peak at 1650 cm^{-1} stemming from the carbonyl of the anion can be seen (Fig. 5b). Parallel to the depoly-
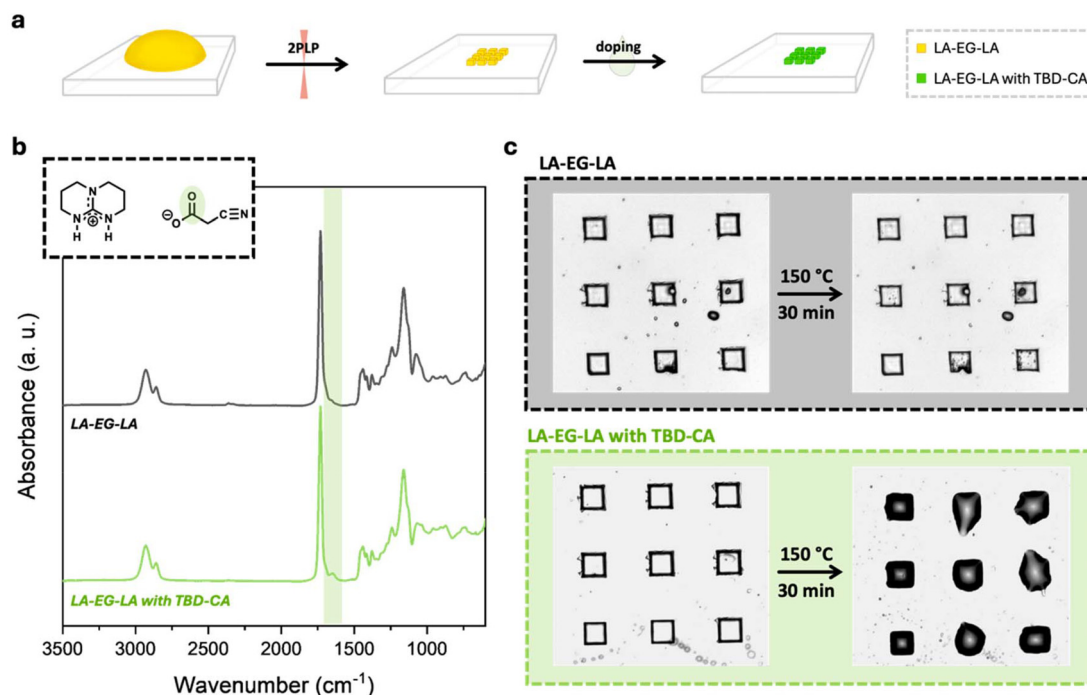
Fig. 5 (a) Schematic representation of the 3D microprinting protocol including latent base incorporation. From left to right: ink droplet (yellow) on a glass substrate for 2PLP, cube array printed with LA-EG-LA, cube array after doping with TBD-CA (green). (b) FTIR spectra showing the difference between doped and blank sample through a latent base peak at 1650 cm^{-1}. (c) Light microscope images before and after heating to 150 °C of micro-printed structures without (top/black, Movie S1) and with (bottom/green, Movie S2) TBD-CA.

merisation experiments on the macro-scale, 3D printed arrays of woodpiles were heated to 150 °C, while being observed under a microscope. The sample containing the latent base clearly shows depolymerisation while the other structures remain unchanged (Fig. 5c and Movies S1, S2), proving the tunability of the process by incorporation of base.

2PLP allows for sequential multimaterial printing by adding fresh ink after the developing step. Thus, we leveraged the potential of this depolymerisable ink on the micro-scale for multimaterial prints. By employing two different materials, depolymerisation conditions can be chosen in such a way, that only one of the printed materials depolymerises. To demon-
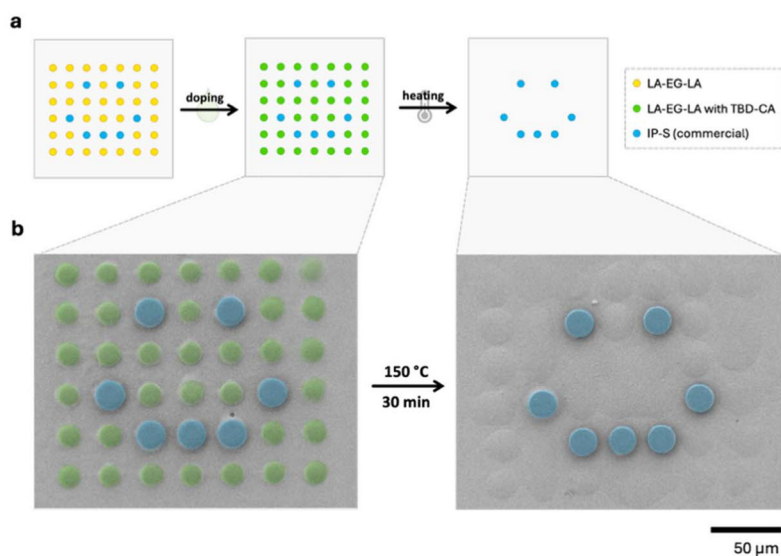

Fig. 6 (a) Schematic representation of the multi-material printing process and the subsequent doping and depolymerisation of the 3D microprinted structures, (b) SEM images of an array of pillars printed with IP-S and LA-EG-LA before and after heating to 150 °C, causing the pillars of LA-EG-LA doped with TBD-CA to depolymerise (subsequently coloured for visual distinction).

strate this with our developed system, an array of pillars (pillars: diameter = 20 μm, height = 10 μm, 7 × 6 array with 10 μm separation) was printed in two steps, using a commercial and non-degradable acrylate-based ink (IP-S, Nanoscribe) and the dithiolane-based LA-EG-LA ink. To visualise the selective depolymerisation, the pillars within the array that were printed with IP-S are arranged to form a smiley face, while the pillars printed with LA-EG-LA fill the rest of the array (Fig. 6a). The latent base was added in a doping step, and the sample was heated to 150 °C. As can be seen in Fig. 6b the pillars that were printed with the dithiolane-based ink and doped with TBD-CA depolymerised, while the commercial ink remained unchanged and the smiley pattern becomes visible. This offers great potential in applications where high resolution and controlled depolymerisation are advantageous, for example as security features or sacrificial materials that can be used as supports.

Conclusion

We developed an acrylate-free ink that shows good 3D printability on both the macro- and micro-scale. The presented system shows the successful implementation of depolymerisation triggered by latent bases for the emerging field of dithiolane-based inks. It further demonstrates a significant advance in adaptable inks in both length scales, while establishing the potential for tuneable thermal depolymerisation. On the micro-scale, the ink proves to print complex geometries with fine features and overhangs at high scanning speeds, outperforming other acrylate-free systems while printing in a comparable range to commercial acrylate-based inks. The present disulfide bonds make this system highly dynamic, while the addition of a latent base to the micro- and macro-printed structures, that can be activated with temperature, allows enhanced thermal depolymerisation. This could be further expanded through integration of latent bases with different triggers into dynamically covalent printed microstructures. The presented approach not only expands on alternative and more sustainable (meth)acrylate-free chemistries for light-based 3D printing but also broadens the application prospects for micro-printed structures through selective depolymerisation.

Experimental section

Materials

All chemicals and solvents were used as received without further purification unless otherwise mentioned. Cyanoacetic acid (CA), N,N'-dicyclohexylcarboiimid (DCC), 4-dimethylaminopyridine (DMAP), lipoic acid (LA) and triazabicyclodecene (TBD) were supplied from TCI. Butylhydroxytoluol (BHT), dichloromethane (DCM), ethyl acetate (EA) and ethylene glycol (EG) were supplied from Merck. Acetone and petroleum ether (PE) were supplied from fisher scientific. Deuterated chloroform (CDCl₃) and deuterated dimethylsulfoxide (DMSO-d₆)

were supplied from Deutero. Sodium sulphate (Na_2SO_4) was supplied from thermo scientific. All procedures were carried out under yellow light conditions.

Synthesis

The full synthetic procedures for LA-EG-LA and TBD-CA are provided in the SI.

^{1}H NMR spectroscopy

^{1}H NMR spectra were recorded on a Bruker Avance III 300 (300 MHz), Avance DRX 300, or Avance III 400 device. Chemical shifts (δ) are reported in ppm in reference to the signal of residual non-deuterated solvent in CDCl₃ or DMSO-d₆.

UV-vis spectroscopy

UV-vis analysis was performed in DCM using a Jasco V-770 Spectrophotometer and a 10 mm cuvette.

Ink preparation

LA-EG-LA was stored under yellow light conditions in DCM with around 50 ppm of BHT relative to LA-EG-LA to avoid polymerisation.

Macro-printing. Prior to printing, the solvent was removed through rotary evaporation. If required, 5 wt% of TBD-CA was added and dissolved by ultrasonication.

Micro-printing. The solvent was removed under Schlenk conditions prior to printing. No further modifications were made.

Digital light processing (DLP)

DLP 3D printing was performed using an Asiga MAX X27 UV DLP 3D printer equipped with an LED light source with a wavelength of 405 nm and a pixel resolution of 27 μm. A custom aluminium build platform with a surface of 25 × 25 mm and a custom aluminium vat were used. The light intensity was fixed at 55 mW cm⁻². After printing the structures were carefully removed from the printing platform with a blade and washed by ultrasonication in isopropanol for 1 min.

Dynamic mechanical analysis (DMA)

DMA was performed on 3D printed strips with dimensions of 20 × 3 × 2 mm using a TA instruments DMA 950 device. The measurements were conducted in a tensile test configuration over a temperature range of −100 to 150 °C with a ramp of 3 °C min⁻¹, a frequency of 1 Hz and an amplitude of 0.01%.

Silanisation procedure

Glass coverslips (22 × 22 mm, 170 μm thickness) were cleaned with isopropanol and acetone and dried with pressurised N₂. The surface was activated by plasma treatment for 30 min. Subsequently the slides were submerged in 4×10^{-3} M solution of 3-(trimethoxysilyl)propyl acrylate in toluene for 3 h. The slides were then washed with toluene and isopropanol and dried with pressurised N₂. The functionalised glass slides were stored under yellow light conditions.

Two-photon laser printing (2PLP)

2PLP was performed on a commercial Photonic Professional GT2 device (Nanoscribe GmbH & Co. KG). All microfabrication was performed with a femtosecond laser (λ = 780 nm) in oil immersion mode focused through a 63× objective (NA = 1.4; WD = 190 µm) supplied from Zeiss. GWL files were created from STL files using the DeScribe software with slicing and hatching set to 300 nm and 200 nm respectively. The laser power and scanning speeds were varied in ranges of 10–35 mW and 2–20 mm s^{-1}, respectively. Coverslips were silanised, attached to commercially available sample holders and the ink was loaded onto the functionalised side of the coverslip. After printing the slides were developed in acetone for 3 min unless otherwise stated.

Latent base doping

A PDMS mould was placed around the microprinted samples. The mould was filled with a solution of TBD-CA in isopropanol (10 mg mL^{-1}) and covered with a circular glass slide. After 30 min the mould was removed, and the glass slide was rinsed with isopropanol and dried with pressurised air.

Fourier-transform infrared (FTIR) spectroscopy

FTIR spectra were recorded on a FTIR microscope (LUMOS-II, Bruker) in attenuated total reflectance (ATR) configuration, 64 scans, with a liquid N$_2$ cooled detector. Arrays of cubes were printed at a scanning speed of 15 mm s^{-1} and a laser power of 15 mW. Before and after doping with the latent base, n = 4 printed structures were measured. The four spectra before and after doping were normalised and averaged.

Light microscopy

Light microscope images of the printed structures were recorded using an Axio Imager 2 microscope (ZEISS Microscopy) equipped with an EC Epiplan-Neofluar 5×/0.13 HD M27 objective and an Axiocam 705 microscope camera. For images at elevated temperatures, a heating stage (LTS 420, Linkam Scientific Instruments) was coupled with the microscope. The temperature ramp was 3 °C min^{-1} until reaching 130 °C and was then reduced to 1 °C min^{-1} until 150 °C were reached. The final temperature was held for 30 min.

Scanning electron microscopy (SEM)

SEM was performed using a Zeiss Supra 55VP (Carl Zeiss AG) instrument at a primary electron energy of 3 keV. Prior to imaging, the printed structures were sputter coated with a 12 nm layer of Pt/Pd (80 : 20) or Pt.

Nanoindentation

Nanoindentation was performed at room temperature using a Bruker Hysitron TI 980 Nanoindenter equipped with a BioXR transducer on cylindrical micropillars printed with dimensions of 60 (d) × 15 (h) µm, or printed bars prepared as mentioned previously for DMA analysis. A 10.26 µm radius conospherical tip made of diamond was employed. Prior to the measurements, the indentation tip was calibrated against air and the tip area function was calculated. All indents were performed in displacement control. An adapted displacement profile based on previous work was employed.[32] After surface detection, the tip was lifted off from the surface to a height of 2000 nm, and finally approached again, to capture the full interaction between the tip and the sample. All samples were indented to a peak displacement of approximately 1000 nm and held for 30 s at maximum displacement as recommended in literature.[33–35] After indentation, the tip was withdrawn from the sample to the same lift-off height. The data were then analysed using the Origin App "Soft Matter Analysis" which belongs to the Bruker's Tribo iQ suite of the technique-specific software applications. The data were then analysed using the Derjaguin–Muller–Toporov (DMT) model. All measurements on microstructures were performed in quadruplicate where possible, while macro-scale structure measurements were performed in triplicate, and the results are shown as mean ± SD.

Conflicts of interest

The authors declare no conflict of interest.

Data availability

The data supporting this article have been included as part of the supplementary information (SI). Raw data for this article are available at the HeiData repository **https://doi.org/10.11588/DATA/LLVDAX**.

Supplementary information is available. See DOI: **https://doi.org/10.1039/d5py00838g**.

Acknowledgements

References

1 S. C. Ligon, R. Liska, J. Stampfl, M. Gurr and R. Mülhaupt, *Chem. Rev.*, 2017, **117**, 10212–10290.
2 R. Su, J. Chen, X. Zhang, W. Wang, Y. Li, R. He and D. Fang, *Small*, 2023, **19**, 2206391.

3 D. L. Bourell, *Annu. Rev. Mater. Res.*, 2016, **46**, 1–18.

4 E. Sanchez-Rexach, T. G. Johnston, C. Jehanno, H. Sardon and A. Nelson, *Chem. Mater.*, 2020, **32**, 7105–7119.

5 V. S. D. Voet, J. Guit and K. Loos, *Macromol. Rapid Commun.*, 2021, **42**, 2000475.

6 A. Jandyal, I. Chaturvedi, I. Wazir, A. Raina and M. U. I. Haq, *Sustainable Oper. Comput.*, 2022, **3**, 33–42.

7 G. A. Appuhamillage, N. Chartrain, V. Meenakshisundaram, K. D. Feller, C. B. Williams and T. E. Long, *Ind. Eng. Chem. Res.*, 2019, **58**, 15109–15118.

8 P. Mainik, C. A. Spiegel and E. Blasco, *Adv. Mater.*, 2024, **36**, 2310100.

9 A. Bagheri and J. Jin, *ACS Appl. Polym. Mater.*, 2019, **1**, 593–611.

10 C. Barner-Kowollik, M. Bastmeyer, E. Blasco, G. Delaittre, P. Müller, B. Richter and M. Wegener, *Angew. Chem., Int. Ed.*, 2017, **56**, 15828–15845.

11 R. Ding, Y. Du, R. B. Goncalves, L. F. Francis and T. M. Reineke, *Polym. Chem.*, 2019, **10**, 1067–1077.

12 J.-T. Miao, S. Peng, M. Ge, Y. Li, J. Zhong, Z. Weng, L. Wu and L. Zheng, *ACS Sustainable Chem. Eng.*, 2020, **8**, 9415–9424.

13 E. M. Maines, M. K. Porwal, C. J. Ellison and T. M. Reineke, *Green Chem.*, 2021, **23**, 6863–6897.

14 D. E. Fagnani, J. L. Tami, G. Copley, M. N. Clemons, Y. D. Y. L. Getzler and A. J. McNeil, *ACS Macro Lett.*, 2021, **10**, 41–53.

15 M. K. Porwal, M. M. Hausladen, C. J. Ellison and T. M. Reineke, *Green Chem.*, 2023, **25**, 1488–1502.

16 A. S. Kuenstler, J. J. Hernandez, M. Trujillo-Lemon, A. Osterbaan and C. N. Bowman, *ACS Appl. Mater. Interfaces*, 2023, **15**, 11111–11121.

17 D. Böcherer, Y. Li, C. Rein, S. Franco Corredor, P. Hou and D. Helmer, *Adv. Funct. Mater.*, 2024, **34**, 2401516.

18 Q. Shi, K. Yu, X. Kuang, X. Mu, C. K. Dunn, M. L. Dunn, T. Wang and H. J. Qi, *Mater. Horiz.*, 2017, **4**, 598–607.

19 S. C. Gauci, P. Somers, M. Aljuaid, M. Wegener, C. Barner-Kowollik and H. A. Houck, *Adv. Funct. Mater.*, 2025, **35**, 2414713.

20 X. Ji, J. Liang, J. Liu, J. Shen, Y. Li, Y. Wang, C. Jing, S. A. Mabury and R. Liu, *Environ. Sci. Technol.*, 2023, **57**, 11704–11717.

21 T. O. Machado, C. J. Stubbs, V. Chiaradia, M. A. Alraddadi, A. Brandolese, J. C. Worch and A. P. Dove, *Nature*, 2024, **629**, 1069–1074.

22 M. A. Alraddadi, V. Chiaradia, C. J. Stubbs, J. C. Worch and A. P. Dove, *Polym. Chem.*, 2021, **12**, 5796–5802.

23 S. Han, V. A. Bobrin, M. Michelas, C. J. Hawker and C. Boyer, *ACS Macro Lett.*, 2024, **13**, 1495–1502.

24 B. R. Nelson, J. T. Cione, B. E. Kirkpatrick, K. M. Kreienbrink, A. P. Dhand, J. A. Burdick, C. Wyatt Shields IV, K. S. Anseth and C. N. Bowman, *Polym. Chem.*, 2025, **16**, 2108–2116.

25 H. Lai, M. L. Dot, J. Chen, J. Zhang and P. Xiao, *ACS Sustainable Resour. Manage.*, 2025, **2**, 833–841.

26 F. Van Lijsebetten, T. Debsharma, J. M. Winne and F. E. Du Prez, *Angew. Chem., Int. Ed.*, 2022, **61**, e202210405.

27 G. Vozzolo, M. Ximenis, D. Mantione, M. Fernández and H. Sardon, *ACS Macro Lett.*, 2023, **12**, 1536–1542.

28 D. Reisinger, M. U. Kriehuber, M. Bender, D. Bautista-Anguís, B. Rieger and S. Schlögl, *Adv. Mater.*, 2023, **35**, 2300830.

29 N. N. Moghal, D. Giannantonio, M. R. Elliott, N. Mehta, A. P. Dove and A. Brandolese, *Faraday Discuss.*, 2025, DOI: **10.1039/D5FD00073D**.

30 P. F. Jacobs, *Rapid Prototyping & Manufacturing, Fundamentals of Stereolithography*, Society of Manufacturing Engineers, Dearborn, 1st edn, 1992.

31 C. Choi, Y. Okayama, P. T. Morris, L. L. Robinson, M. Gerst, J. C. Speros, C. J. Hawker, J. Read De Alaniz and C. M. Bates, *Adv. Funct. Mater.*, 2022, **32**, 2200883.

32 O. Eivgi, C. Vazquez-Martel, J. Lukeš and E. Blasco, *Small Methods*, 2025, 2500432.

33 J. C. Kohn and D. M. Ebenstein, *J. Mech. Behav. Biomed. Mater.*, 2013, **20**, 316–326.

34 R. Srinivasaraghavan Govindarajan, S. Sikulskyi, Z. Ren, T. Stark and D. Kim, *Polymers*, 2023, **15**, 4377.

35 T. Koch, W. Zhang, T. T. Tran, Y. Wang, A. Mikitisin, J. Puchhammer, J. R. Greer, A. Ovsianikov, F. Chalupa-Gantner and M. Lunzer, *Adv. Mater.*, 2024, **36**, 2308497.